Applied Catalysis B: Environmental 126 (2012) 290–297

Contents lists available at SciVerse ScienceDirect

Applied Catalysis B: Environmental

journal homepage: www.elsevier.com/locate/apcatb

Exploring the relationship between surface structure and photocatalytic activity of flame-made TiO_2-based catalysts

Yijiao Jiang, Jason Scott, Rose Amal*

ARC Centre of Excellence for Functional Nanomaterials, School of Chemical Engineering, The University of New South Wales, Sydney, NSW 2052, Australia

ARTICLE INFO

Article history:
Received 16 April 2012
Received in revised form 21 June 2012
Accepted 24 July 2012
Available online 1 August 2012

Keywords:
Photodegradation
Acetaldehyde
Titanium dioxide
Dopants
Flame spray pyrolysis
Surface hydroxyl groups
^{1}H MAS NMR

ABSTRACT

Bare titanium dioxides (TiO_2) and doped with metal (Cu) or non-metal ion (F) were synthesized by a single-step flame spray pyrolysis (FSP) method. According to the BET, XRD, and TEM results, the Cu- and F-doped TiO_2 nanoparticles synthesized by FSP possess comparable features in terms of surface area, crystallite size and phase composition, and morphology. However, the F-doped TiO_2 exhibited the highest photocatalytic activity for the complete oxidation of acetaldehyde (ACE) even surpassing benchmarking Aeroxide TiO_2 (P25). In contrast, Cu-doped TiO_2 had a detrimental effect on the ACE photocatalytic oxidation. The proportion of native terminal hydroxyl groups, evaluated using high-field ^{1}H MAS NMR, on the particle surface was varied by doping the TiO_2 with either Cu or F ions during FSP synthesis. A relationship, whereby decreased terminal hydroxyl group content corresponded to elevated acetaldehyde photodegradation, was subsequently uncovered. The findings were reinforced by studying the XPS O 1s photopeaks in the region attributed to surface hydroxyl groups.

1. Introduction

Heterogeneous photocatalytic oxidation (PCO) is a promising technology that can be envisaged to remove low concentrations of volatile organic compounds (VOCs) at room temperature by totally oxidizing them to CO_2 and H_2O in an environmentally benign manner [1]. On the other hand, photodegradation of gaseous acetaldehyde (ACE) has been often used as a model reaction for screening PCO activities of different photocatalytic materials [2]. ACE is also known as a representative indoor air pollutant and one of the most abundant carbonyl compounds in the atmosphere. Titanium dioxide (TiO_2) is the most prominent photocatalyst because of its low cost, non-toxicity, and abundance [3]. However, its commercial application is hindered by the low quantum efficiency and poor understanding of the structure–reactivity relationships. Correlations between structure and photoactivity have been proposed with much effort devoted to developing active TiO_2-based photocatalysts with enhanced structural properties including crystallinity, crystallite size and phase, surface area, morphology, and surface modification by doping metals/anions [4–6]. Conjecture remains over those properties which contribute the most to the activity or whether unknown factors, directly related to the photocatalytic activity, still exist.

Generally, heterogeneous photocatalysis is initiated and occurs on the surface of a solid semiconductor. It is well known that the outermost surface of an oxide is covered with a layer of hydroxyl groups [7]. The nature of these surface hydroxyl groups is of great importance in governing the surface reaction that ensues. For example, the acid–base properties determine the surface charge and influence the interaction between polar organic molecules and oxide surfaces [8], and may play a considerable role in photocatalytic oxidation of organic compounds. It has been reported that post-treatment of TiO_2 with Brønsted acids such as sulfuric acid or hydrofluoric acid led to much higher photocatalytic activity [9,10]. To the best of our knowledge, the role of the intrinsic hydroxyl groups present on the surface of TiO_2 in defining the photocatalytic activity has not been explored so far, and this understanding will trigger additional optimization of existing photocatalysts and the rational design of new ones.

Photocatalyst preparation and/or post-treatment using different methods (such as sol–gel or precipitation) or under different conditions (acid or base treatment) can influence structural properties and surface hydroxyl group distribution, as they are very sensitive to the local environment. Herein, flame spray pyrolysis (FSP) has been used to controllably synthesize TiO_2-based materials with minimal variation to the above-mentioned structural properties. FSP itself is emerging as an attractive fast and single-step catalyst preparation method [11–13]. F- and Cu-doped TiO_2 have been previously used for oxidizing VOCs [14–18]. In this study, bare TiO_2 nanoparticles and TiO_2 doped with F or Cu prepared by FSP were used to study the photocatalytic oxidation of

* Corresponding author. Tel.: +61 2 9385 4361; fax: +61 2 9385 5966.
E-mail address: r.amal@unsw.edu.au (R. Amal).

0926-3373/$ – see front matter © 2012 Elsevier B.V. All rights reserved.
http://dx.doi.org/10.1016/j.apcatb.2012.07.027

low concentration ACE as a model compound. Prior to the photocatalytic activity test, all the catalysts were fully characterized by BET, XRD, TEM measurements. The results were compared with the widely accepted benchmark photocatalyst Aeroxide TiO_2 (P25). Due to the atomic specificity and quantitative capabilities, ^1H magic angle spinning (MAS) NMR, proven to be a powerful technique for characterizing surface hydroxyl groups [19], was employed to characterize the surface hydroxyl groups present on the TiO_2-based photocatalysts, as well as study the crucial relationship between surface structure and photocatalytic activity.

2. Experimental

2.1. Catalyst preparation

Titanium tetraisopropoxide (TTIP, Aldrich, 97%), hexafluorobenzene (Aldrich, 99%), copper (II) 2-ethylhexanoate (Aldrich, 99.9%), xylene (analytical grade, Univar), and acetonitrile (analytical grade, Fluka) were used as received. Commercial Aeroxide P25 TiO_2 was purchased from Degussa. Bare TiO_2 and TiO_2 doped with F or Cu ions were prepared by one-step FSP. The experimental set-up used for FSP has been described in detail elsewhere [20]. In brief, flame-made bare TiO_2, 50 at% F-TiO_2, and 2 at% Cu-TiO_2 nanoparticles were prepared by dissolving the given amounts of precursor materials in a mixture of xylene/acetonitrile with a volume ratio of 1:1. The resulting solution was filtered over a glass filter, then fed to the flame through a syringe pump at 5 mL/min and dispersed by 5 L/min of O_2 at 1.5 bar. The resulting spray was ignited by an annular supporting methane/oxygen flame (1.5/3.2 L/min) resulting in an approximately 6 cm long flame. Nanoparticles were collected on a cooled fibre glass filter (Whatmann GF6, 257 mm in diameter) by assistance of a vacuum pump (Alcatel SD series).

2.2. Textural and morphological properties

The Brunauer–Emmett–Teller (BET) surface area and pore size of the materials were obtained from nitrogen physisorption isotherms (adsorption–desorption branches) at 77 K on a Micromeritics Tristar 3000 instrument. Before the BET measurement, the samples were degassed overnight under vacuum at 150 °C to vaporize water molecules adsorbed on the material.

X-ray diffraction (XRD) patterns were recorded on a Philips X'pert Multipurpose X-ray Diffraction System using Cu $K\alpha_1$ (λ = 1.5406 Å) radiation in step mode between 22° and 85° 2θ with a step size of 0.026° and 50 s per step. An array detector with 255 cells was used. The X-ray operating conditions were 45 kV and 40 mA. Metallic Cu was used as an internal standard.

For high-resolution transmission electron microscopy (HRTEM), specimens were prepared by ultrasonically suspending the materials in ethanol and a few drops were deposited onto a perforated carbon foil supported on a copper grid. HRTEM investigations were performed on a Philips CM200 microscope (FEI; LaB_6 cathode, operated at 200 kV, point resolution ~2 Å). Scanning electron microscope (SEM) images were obtained on a FEI Nova NanoSEM 230 FESEM equipment. A chromium-sputter coating was used for high resolution SEM.

2.3. Photocatalytic activity test

Photocatalytic oxidation of gaseous ACE on FSP-made TiO_2-based photocatalyts was carried out in a continuous-flow packed bed annular glass photoreactor illuminated by four surrounding lamps (NEC FL6BL-B UV-A lamps, 6 W, λ_{max} = 355 nm), described in detail elsewhere [21]. The annular reactor consisted of a closed 11.1 mm diameter glass tube inserted into an open ended glass tube (11.3 mm ID, 15.0 mm OD), which gave an average annular spacing of 0.1 mm width. The four lamps were symmetrically positioned around the photoreactor with separation distance of 5 cm. This setup was housed within a UV black box, which was fitted with a fan to dissipate the heat generated by the lamps, thus ensuring the adsorption capacity was not influenced by a rise in temperature.

Gas flows were regulated by mass flow controllers (Brooks Instrument B. V., model 5850E). Typically, 20 mg of photocatalyst was diluted with 240 mg of silica beads (100 μm diameter) and kept in place between two quartz wool plugs. Initially, dry air (Coregas, 28.9 mL/min) was passed through the photoreactor under UV illumination to photodegrade any residual organic impurities on the catalyst surface. The presence of impurities was assessed by CO_2 levels in the reactor effluent with a negligible level of CO_2 indicating all impurities had been removed from the catalyst bed. Prior to photocatalytic oxidation, a stream with an ACE concentration of 183 ± 10 ppm combining ACE (Coregas, compressed in Argon) and air was co-fed over the catalyst without illumination until saturation was achieved. Once the catalyst was saturated with ACE, photocatalytic oxidation was commenced with the four lamps turned on after an initial sample had been taken. Control experiments indicated no ACE degradation occurred when ACE was passed through the photoreactor either with illumination but no photocatalyst or containing photocatalyst but with no illumination. Photocatalyst saturation by ACE prior to illumination was determined by periodically (every 10 min) sampling the photoreactor effluent stream until a consistent ACE concentration was attained. ACE and CO_2 concentrations in the photoreactor effluent were analyzed using an on-line gas chromatograph (GC, Shimadzu 2010) with a flame ionization detector (FID) and methanizer. The GC was equipped with a HP-PLOT/Q capillary column (length 30 m, inner diameter 0.32 mm, Agilent Technologies). The products were calibrated against a calibration gas mixture.

2.4. Surface chemical bonding characterized by XPS

Surface analysis by XPS was performed using an ESCALAB250Xispectrometer (Thermo Scientific, UK) employing a mono-chromated Al Kα (1486.68 eV) X-ray source operated at 15.2 kV and 168 W (10.8 Ma). The photoelectron take-off angle was 90° measured with respect to the surface of the sample. Typical operating pressure in the vacuum chamber was $\sim 2 \times 10^{-9}$ Torr. Survey (wide-scan) spectra were obtained with pass energy of 100 eV. Surface narrow-scan spectra with pass energy of 20 eV were obtained for the C 1s, O 1s, Ti 2p, and F 1s photopeaks. The line shapes used for curve fitting were pure Gaussian, and integrated background was employed. All binding energies were referenced to the carbon C—H photopeak at 285.0 eV. In addition, F-doped TiO_2 was sputtered using an argon sputtering gun operated at 3.0 kV and 25 mA, and a pressure of 10 mPa to give a nominal sputtering rate of 5 Å/min.

2.5. Surface hydroxyl groups determined by ^1H MAS NMR

^1H MAS NMR experiments were performed on a Bruker Avance III 700 spectrometer at a resonance frequency of 700.36 MHz for ^1H nuclei. Single-pulse excitation corresponding to a $\pi/2$ flip angle with repetition time of 1 s was used. An ultrahigh-speed 2.5 mm Bruker MAS probe at a sample spinning rate of 25 kHz was used. Typically, 128 transients were acquired using a small pulse angle (2.1 μs pulse width). The chemical shifts were measured relative to 4, 4-dimethyl-4-silapentane-1-sulfonic acid (DSS) as an external standard. The solid-state NMR spectra were processed using the Bruker software TOPSPIN 3.0. The as-synthesized samples were directly used after FSP without any further treatment.

Table 1
BET specific surface area (SSA), isotherm type, and anatase percentage for bare and doped FSP-made TiO_2 as measured by N_2 adsorption and XRD.

Samples	SSA (m^2/g)	Isotherm type	Anatase %
bare TiO_2	85	IV	80
F-TiO_2	55	IV	78
Cu-TiO_2	47	IV	73

3. Results and discussion

3.1. Textural and morphological properties

As previously demonstrated, the one-step FSP method can be used to prepare TiO_2 nanoparticles with controlled specific surface area (SSA), crystallite size and phase [22,23]. To minimise complexities in this study, TiO_2 nanoparticles with similar physical properties to P25 were synthesized by the FSP method. Xylene, with a significantly high combustion enthalpy (~4600 kJ mol^{-1}), was used as the solvent to ensure a high enthalpy density in the flame and particle formation *via* nucleation from the gas phase [24]. Moreover, the O_2 pressure drop was adjusted to 1.5 bar for high dispersion of the liquid precursor spray. As shown in Table 1, the FSP-made bare TiO_2, F-TiO_2, and Cu-TiO_2 possess BET SSAs (from N_2 adsorption) in the range of 47–85 m^2/g. This range of values also encompasses the SSA of Aeroxide P25 TiO_2 (50 m^2/g). On comparison with bare TiO_2, a mild reduction in surface area was observed for the catalysts doped with different atoms (55 m^2/g for F-TiO_2 and 47 m^2/g for Cu-TiO_2). This was attributed to metal/anion sintering residues on the surface of TiO_2. A similar SSA effect was observed by Huang et al. when additional metals were added to FSP-made Pd/SiO_2-Al_2O_3 [12]. Nitrogen adsorption–desorption isotherms (not shown here) for each of the FSP-made TiO_2-based nanoparticles exhibited Type IV character which is typical for non-porous flame-made materials.

Crystallinity and crystal phase are important parameters which influence photocatalyst behavior. It is well-accepted that a highly crystalline TiO_2 structure is required to achieve high photocatalytic activity. The XRD patterns of the TiO_2-based nanoparticles are displayed in Fig. 1. The spectra suggest the samples are completely crystalline as no amorphous humps could be found in the wide-angle XRD pattern. They all contain diffraction peaks at 2θ = 25, 37, 38, and 48° which can be attributed to the anatase crystal planes of (1 0 1), (1 0 3), (0 0 4), and (2 0 0) and are in good agreement with JCPDS file No. 21-1272. Clear reflections at approximately 2θ = 27°, 36°, and 55° correspond to the (1 1 0), (1 0 1), and (2 1 1) crystal planes of rutile, also in good agreement with JCPDS file No. 21-1276. It has been demonstrated by others as well as our own work that a mixture of anatase and rutile in the particles can enhance photocatalytic activity [5,25,26]. No reflections representing the brookite phase were observed in any of the catalysts. An anatase to rutile phase ratio of approximately 4:1 (Table 1, final column) was determined from crystallite phase analysis (using High Score plus software with the ICDD database). Importantly, they possess a phase composition similar to Aeroxide P25, which comprises 83% anatase and 17% rutile.

Often the morphology of a sample can influence its chemical properties as well. Typical TEM images of the FSP-made TiO_2-based nanoparticles are shown in Fig. 2. The TEM pictures of bare and doped TiO_2 indicate the particle diameters are in the range of 5–20 nm, with a majority of the TiO_2 particles being below 10 nm. The presence of Cu nanoparticles in the Cu-doped TiO_2 sample was verified by EDX (not shown). Studies by Teoh et al. found anatase and rutile existed as separate crystallites in FSP-made TiO_2 particles [22]. As anatase is the dominant crystallite phase (from XRD), the smaller spherical particles might be anatase, while the larger

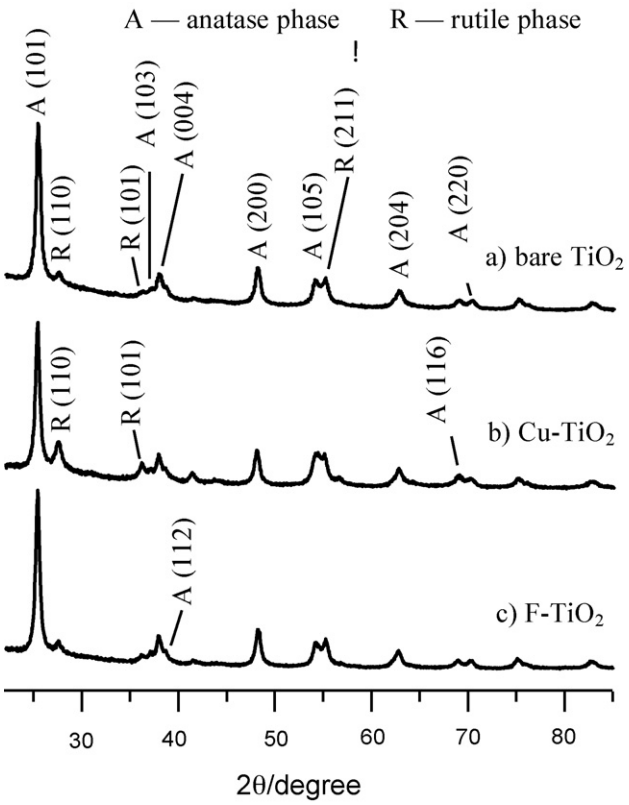

Fig. 1. Powder XRD patterns of (a) bare TiO_2, (b) Cu-TiO_2, and (c) F-TiO_2.

ones could be rutile. However, discerning between anatase and rutile crystallinity using TEM is difficult due to the small differences in lattice spacing. Similarly, the TEM images of Aeroxide P25 recorded by Ohno et al. showed that both anatase and rutile particles exist separately from their studies [25]. The SEM image of F-TiO_2 (Fig. 2d) clearly shows the FSP method provided very uniform fluorinated nanoparticles. To briefly summarize, the Cu- or F-doped TiO_2 nanoparticles synthesized by FSP exhibit comparable structural properties in terms of crystallite size, phase composition, and morphology evidenced by the BET, XRD, and TEM results.

3.2. Photocatalytic activity

In this study, Aeroxide P25 TiO_2, commercially produced by vapour-fed flame synthesis, was used as the benchmark photocatalyst. ACE photodegradation was conducted in a continuous-flow packed bed annular glass photoreactor under UV light irradiation. Prior to photocatalytic oxidation, the ACE concentration in the effluent was plotted as a function of dark adsorption time as shown in Fig. S3. The adsorption isotherm slope of F-TiO_2 was larger than that of bare TiO_2 and Cu-TiO_2. It indicates that F-TiO_2 showed faster adsorption rate, while bare TiO_2 and Cu-TiO_2 provided a slow-down equilibrium course. It implies that the number of adsorption sites is thought to be less on bare TiO_2 and Cu-TiO_2. Once the catalyst was saturated with ACE, photocatalytic oxidation was commenced with the four lamps turned on. Fig. 3 depicts the photodegradation profile of ACE removal and CO_2 formation as a function of irradiation time. The initial ACE concentration was 183 ± 10 ppm. Upon UV illumination, the ACE concentration in the effluent rapidly declined for all the studied photocatalysts. The FSP bare TiO_2 profile showed 40 ppm ACE remained after photodegradation, corresponding to 78% of ACE removal. Cu-doped TiO_2 displayed minor photocatalytic activity (~12% ACE removal), whereas F-doped TiO_2 resulted in a

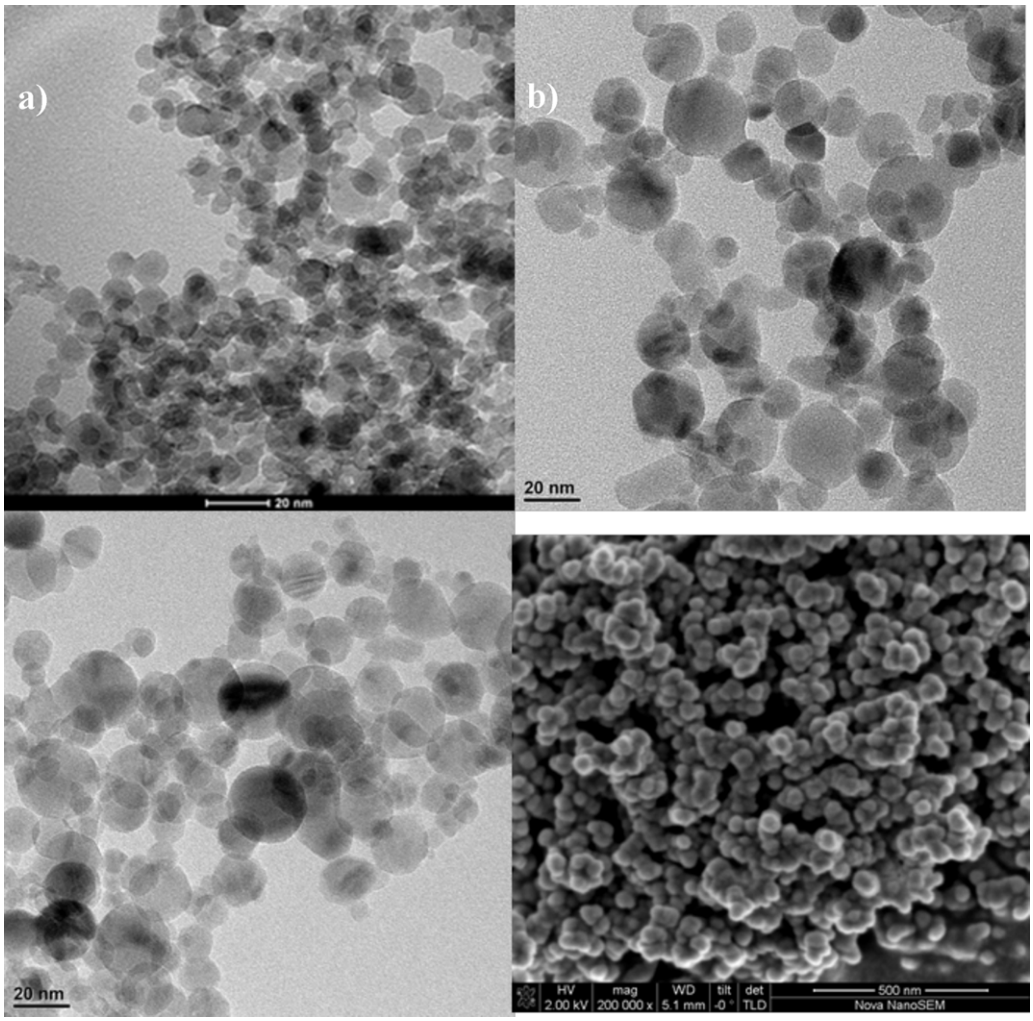

Fig. 2. TEM images of (a) bare TiO_2, (b) Cu-TiO_2, (c) F-TiO_2, and (d) SEM image of F-TiO_2.

significant activity enhancement (up to 97%) of ACE removal. This slightly exceeded that of P25 (93%).

Photocatalyst deactivation is frequently related to the build-up of unreactive by-products on the active sites of the surface. As shown in Fig. 3b, CO_2 was observed as the primary gaseous product escaping from all the photocatalysts used in this study. For the F-TiO_2, approximately 520 ppm of CO_2 was initially evolved, which exceeded stoichiometric CO_2 production, *i.e.* 2[ACE]. This can be attributed to initial CO_2 generation deriving not only from gaseous ACE but also ACE pre-adsorbed on the catalyst surface. The initial CO_2 peak also indicates the UV light intensity is sufficient so as not to restrict the gaseous acetaldehyde removal rate. If light intensity was governing photoactivity then this peak would not appear. At steady state, the mass balance between ACE and CO_2 was within ±10% which indicates near quantitative conversion was achieved. The F-TiO_2 was able to maintain the high level of ACE photodegradation over more than five days (not shown) with no deactivation observed in the present study, indicating this photocatalyst possesses a long life time. However, it is possible if the concentration of acetaldehyde was too high, the concentration of adsorbed intermediates on the surface could potentially limit the access of reactive molecules to the adsorption sites. Under these circumstances, a decrease of the conversion would be expected. However, no intermediates were detected in the gas phase. This behavior indicates the intermediate desorption rate was lower than their photocatalytic oxidation rate.

It is apparent the Cu dopant had a detrimental effect on photocatalytic performance. The color change was observed in the oxidation process on Cu-TiO_2, which can be explained that Cu oxides react with the TiO_2 photogenerated electrons. Thus, the electron reaction with the adsorbed O_2 molecules may be decreased and hence the reaction of O_2^- radicals that yield acetate. It indicates that the presence of Cu on TiO_2 did not improve electron/hole separation and did not allow for efficient photogenerated electron trapping. This finding differs from a previous claim whereby the addition of Cu promoted charge separation and inhibited photo-excited electron and hole recombination, therefore enhancing photocatalytic activity [27]. A possible cause of the alternate behavior may be the different methods of photocatalyst preparation. Unlike the conventional multistate solution-based method, Cu species prepared by the one-step FSP are enriched and highly surface-dispersed on the TiO_2 as demonstrated in our earlier work [16,28]. Similarly, the F ions were enriched on the TiO_2 surface, as evidenced by the binding energy of 682 eV in the XPS F 1s depth profile (Fig. 4), but as opposed to Cu imparted a beneficial outcome. Both Cu-TiO_2 and F-TiO_2 samples exhibited negligible change in optical absorption in comparison with bare TiO_2 and Aeroxide P25, as shown in Fig. S1.This variation in performance leads to questions concerning the origins of the photoactivity in this instance. There might be some unknown properties which may directly determine the activity.

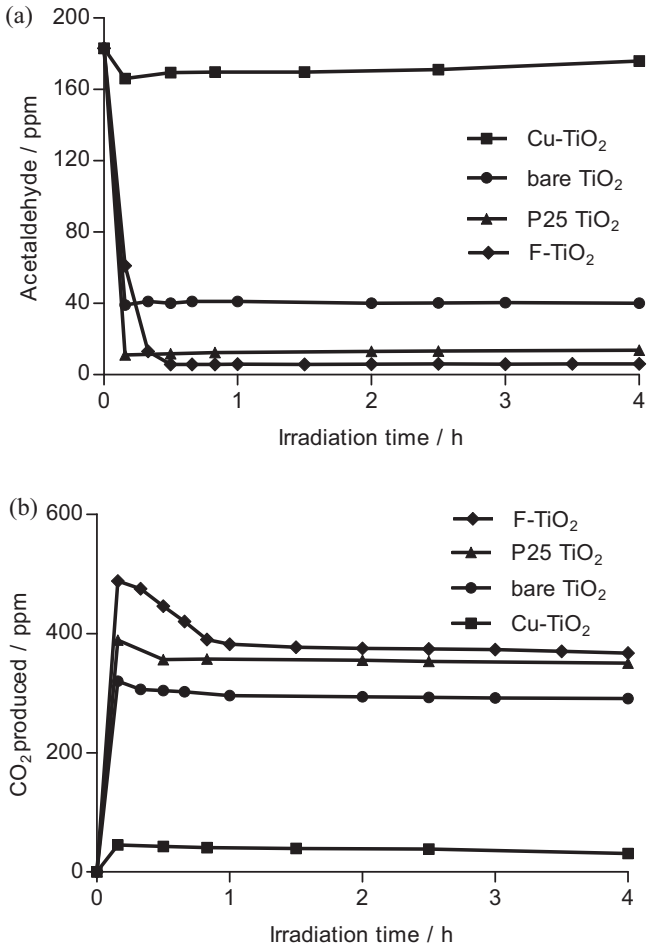

Fig. 3. (a) UV photodegradation profiles of ACE and (b) corresponding CO_2 production from ACE photodegradation using the FSP-made TiO_2 compared to Aeroxide P25. Initial ACE concentration = 183 ± 10 ppm.

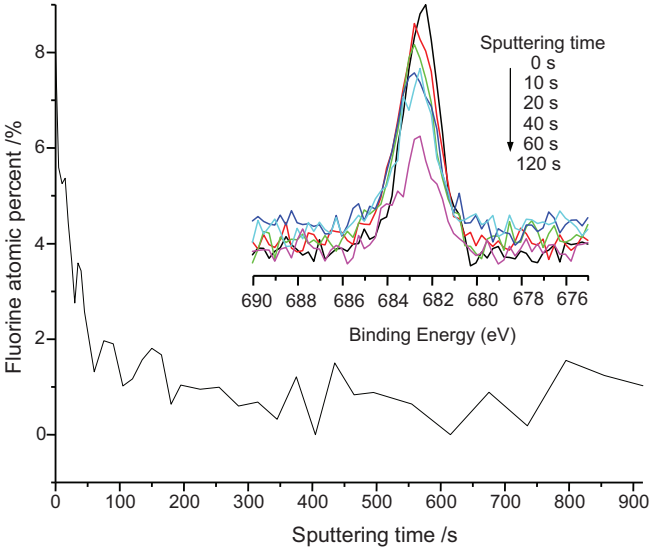

Fig. 4. Fluorine atomic percent in the FSP-made F-doped TiO_2 as a function of particle depth, expressed in terms of sputtering time. The inset shows the depth profile of the XPS spectra using a sputtering argon ion beam at various times.

The BET, XRD, and TEM results indicated that the bulk crystal structure and morphological properties of the FSP-made TiO_2 were not considerably altered by varying the type of dopant atoms (either Cu or F). Since solid-catalyzed heterogeneous photoreactions take place on the surface of a photocatalyst, surface structure is anticipated to affect reaction efficiency as well. It has been reported that fluorination is a very effective means to increase the surface acidity of TiO_2 arising from the strong electronegativity of fluorine [29]. Based on this, the enhanced photocatalytic activity of ACE on F-doped TiO_2 is likely attributed to the surface structure.

3.3. Surface chemical bonding characterized by XPS

To understand the origin of the elevated photocatalytic activity of the FSP-made F-TiO_2, we firstly examined the change in surface chemical bonding of the TiO_2 photocatalysts by XPS, which has been often used as a sensitive method to study the surface state of a material. Fig. 5 shows a typical XPS survey (wide-scan) spectra of the FSP-made bare TiO_2 and F-TiO_2. Obviously, Ti, O, and C elements with comparable peak intensities were present at the surface of both the bare and F-doped TiO_2 samples. The photoelectron peaks of Ti 2p, O 1s, and C 1s are clearly present at binding energies of 457, 530, and 285 eV, respectively [7]. In Fig. 6, the Ti 2p XPS spectra are identical for both the bare and F-doped TiO_2,

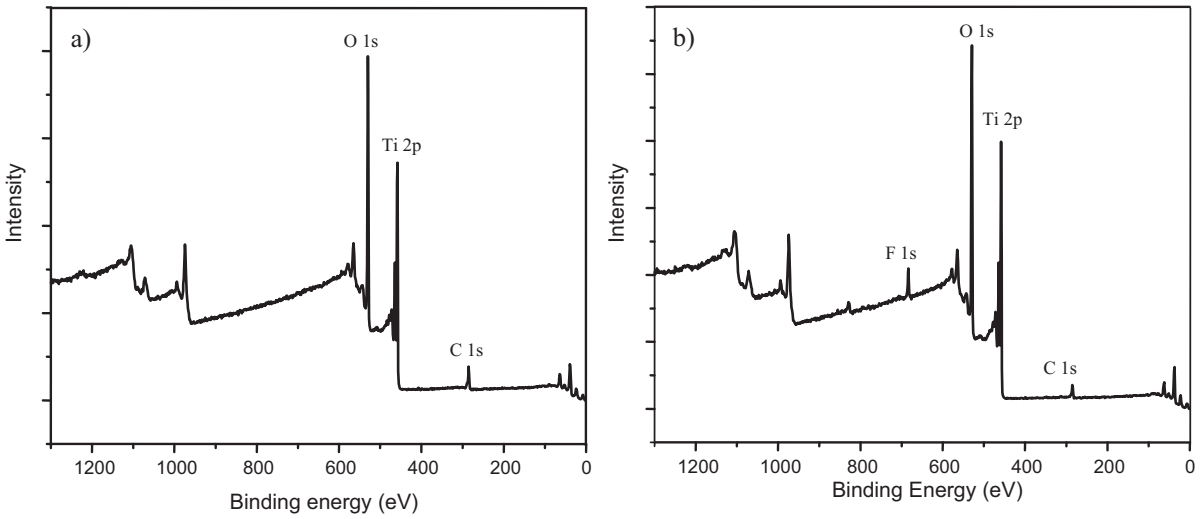

Fig. 5. XPS survey spectra of the FSP-made (a) bare TiO_2 and (b) F-doped TiO_2.

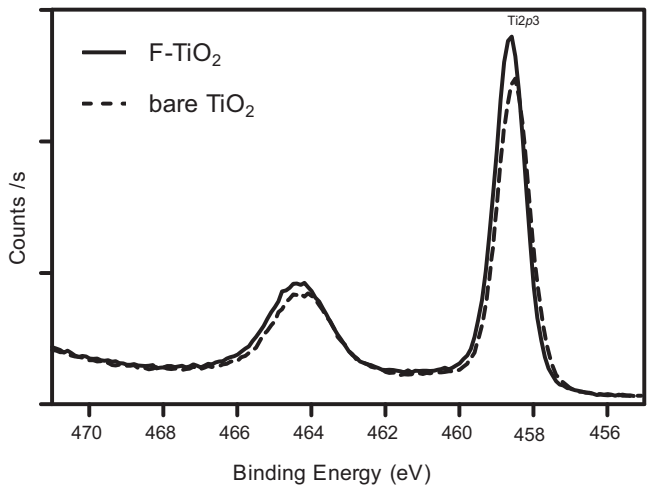

Fig. 6. Ti 2p XPS spectra for the FSP-made bare TiO_2 (dashed) and F-doped TiO_2 (solid) over the binding energy range of 455–471 eV.

which indicates that Ti atoms have a similar bonding environment after fluorine doping by FSP synthesis and does not resemble Ti 2p XPS spectra of TiO_2 doped with nitrogen [30]. It was found that C elements with comparable peak intensities were present on the surfaces of both the bare and F-doped TiO_2 samples (not shown).

Fig. 7 depicts XPS narrow-scan in the O 1s element region over a binding energy range of 526–535 eV for the bare and F-doped TiO_2. The O 1s peaks were deconvoluted into three individual photopeaks assigned to the oxygen species O^{2-} (O 1s A), hydroxyl groups (O 1s B) and chemisorbed water OH (O 1s C) from the lowest to the highest binding energy, respectively. For F-TiO_2, the O 1s peak showed a declined shoulder at the regions of O 1s B and O 1s C attributed to hydroxyl groups and chemisorbed water, respectively. This finding indicates F-TiO_2 may contain less hydroxyl groups as compared to the bare TiO_2. However, since most oxygen-containing functional groups such as C—O and O—C=O species also give approximate O 1s binding energies of 532 eV, or exist at the same location as the hydroxyl groups in the O 1s XPS spectrum, it is necessary to correct the O 1s photopeaks for contributions from surface hydroxyl groups by ^{1}H MAS NMR.

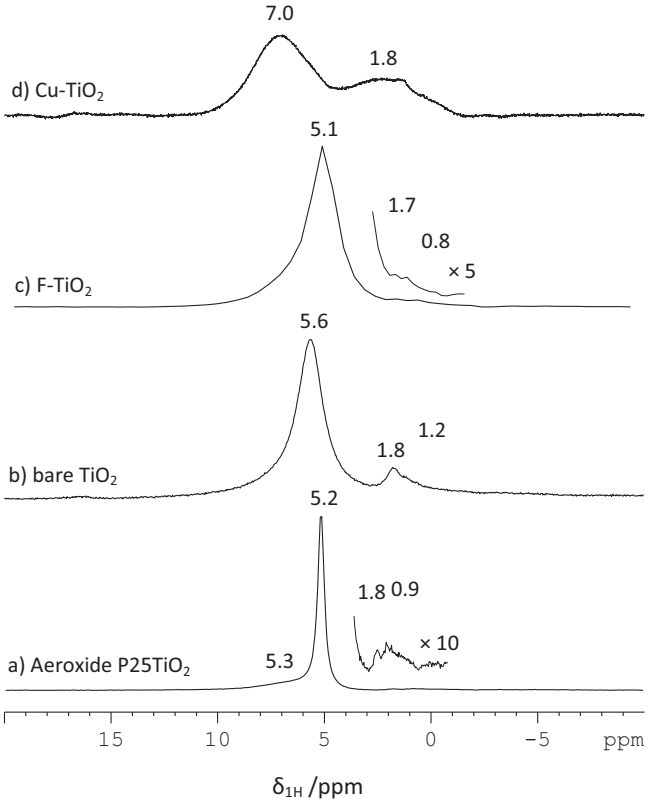

Fig. 8. ^{1}H MAS NMR spectra of (a) Aeroxide P25 TiO_2, (b) bare TiO_2, (c) F-TiO_2, and (d) Cu-TiO_2.

3.4. Surface hydroxyl groups determined by ^{1}H MAS NMR

^{1}H MAS NMR has been proven to be a powerful technique for characterizing surface hydroxyl groups [19]. The ^{1}H MAS NMR spectra for the FSP-made TiO_2-based nanoparticles and P25 TiO_2 are shown in Fig. 8. The spectrum of P25 exhibits a main signal at 5.2 ppm, which is assigned to the bridging hydroxyl groups (bridging TiOH) as described in Scheme 1. Previous studies have proven the bridging hydroxyl groups possess acidic properties [10,31,32]. By enlarging the P25 NMR spectrum, closer inspection of the spectra reveals two very weak signals at *ca.* 1.8 and 0.9 ppm, which can

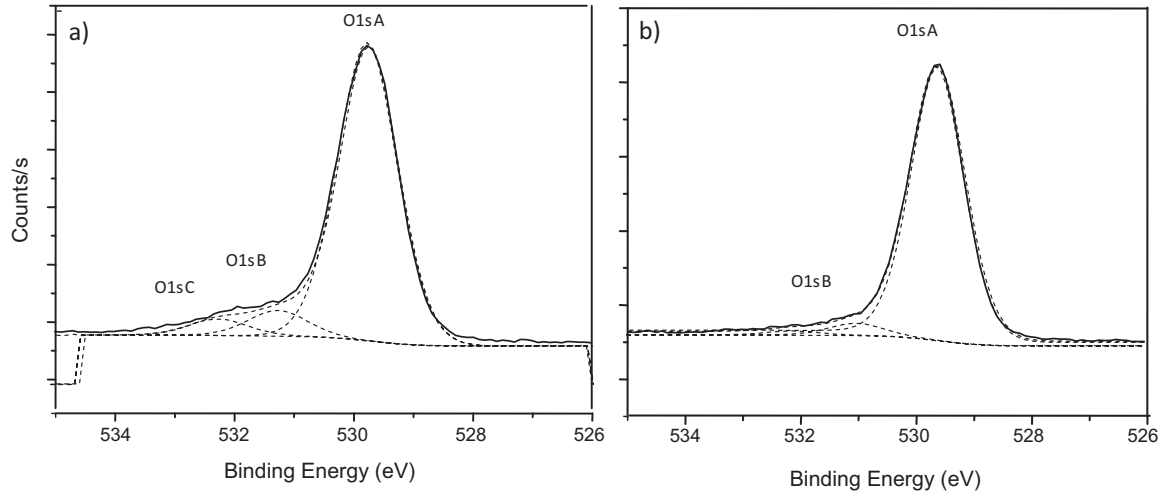

Fig. 7. O 1s XPS spectra for the FSP-made bare (a) TiO_2 and (b) F-doped TiO_2 over the binding energy range 526–535 eV. Spectra include deconvoluted peaks identifying O atoms coordinated with titanium.

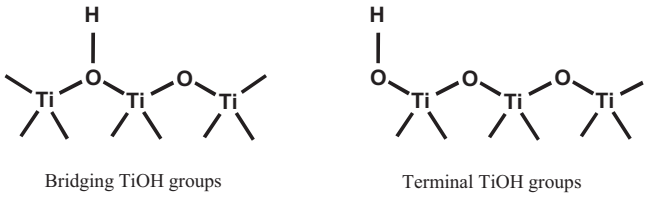

Scheme 1. Schematic of bridging TiOH groups and terminal TiOH groups.

be attributed to terminal hydroxyl groups (terminal TiOH, shown in Scheme 1) in the anatase phase and rutile phase, respectively [33]. This finding demonstrates the supremacy of ^{1}H MAS NMR in distinguishing anatase and rutile phase, since it was not possible to differentiate these phases by HRTEM due to small differences in lattice spacing. Terminal hydroxyl groups have been described as basic in character, as evidenced by the fact that they undergo exchange with fluoride ions [31]. The signal intensity ratio of bridging and terminal TiOH groups in the Aeroxide P25 TiO_2 is about 23:1.

In the case of the bare FSP TiO_2 (Fig. 8b), the peaks at approximately 1.8 and 1.2 ppm and ascribed to the basic terminal TiOH groups of anatase and rutile, respectively, are much more pronounced. The signal positions of the acidic bridging TiOH groups in the bare TiO_2 shift to lower fields at 5.6 ppm. This shift might be due to small amounts of physisorbed and chemisorbed water. In Fig. 8c, F-TiO_2 provided a significant decrease in the intensity of terminal TiOH groups compared to the bare FSP TiO_2. The signal intensity ratio of bridging and terminal TiOH groups in this instance is about 25:1. This fact suggests that during FSP synthesis an exchange between surface hydroxyl groups on the TiO_2 and fluorine atoms in the hexafluorobenzene might occur. The basic terminal TiOH groups were substituted preferentially as evidenced by the considerable reduction of terminal TiOH groups. Compared to F-TiO_2, Cu-TiO_2 provided a much higher intensity of terminal hydroxyl groups. It is also noted the line width becomes much broader due to the existence of paramagnetic Cu(II) species and presents clear evidence of the interaction between Cu atoms and TiO_2 within the particles. Interestingly, the findings show when the relative content of terminal TiOH groups is higher (*ca.* 30% in Cu-TiO_2), meaning a considerable number of basic sites are present on the surface, the lowest ACE photodegradation is observed (Fig. 3a).

This is illustrated clearly in Fig. 9 which compares the ACE concentration (squares) in the effluent after UV photodegradation and CO_2 produced (triangles) under the steady-state conditions as a function of relative content of terminal TiOH groups (from Fig. 8). The minimum ACE concentration of 6 ppm after

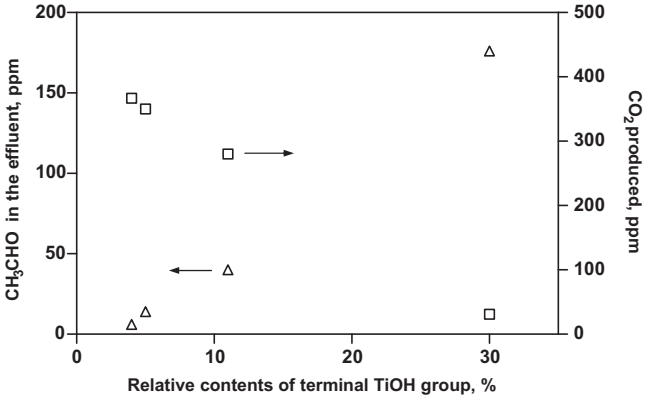

Fig. 9. Variation of the ACE concentration after UV photodegradation (ACE in the effluent, cubes) and CO_2 produced (triangles) under steady-state conditions with the relative content of terminal TiOH groups estimated by ^{1}H MAS NMR studies. Initial ACE concentration = 183 ± 10 ppm.

photodegradation is observed for F-TiO_2 containing a minimum number of terminal TiOH groups (*ca.* 4%). The CO_2 produced strongly decreased with increasing content of terminal TiOH groups. Similarly, the signal representing terminal hydroxyl groups in P25 was minor and may be a factor contributing to its comparative photoactivity with F-TiO_2. On maintaining comparable surface areas, crystallite sizes and phase compositions, and morphology, it is apparent the surface hydroxyl group distribution plays a key role in determining photocatalytic activity. The low content of surface terminal hydroxyl groups present in F-TiO_2 may promote better photo-induced charge carrier separation, and thus favor the UV photodegradation of gaseous ACE.

Anpo and co-workers observed that the photocatalytic activity of TiO_2/ZSM-5 for the oxidation of ACE strongly depended on the SiO_2/Al_2O_3 ratio of the ZSM-5 zeolites. It is well established that a higher SiO_2/Al_2O_3 ratio leads to a stronger Brønsted acid site [34], which is beneficial for photoactivity. Very recently, Zhao and co-workers found the photocatalytic oxidation of alcohols on TiO_2 could be dramatically accelerated by simple pretreatment of TiO_2 with Brønsted acids such as sulfuric acid and hydrofluoric acid [9]. Instead of necessitating additional acid treatment of the surface as reported above, the present work has found the photocatalytic activity can be elevated simply by changing the intrinsic distribution of native hydroxyl groups present on the TiO_2 surface.

4. Conclusions

Bare TiO_2 and TiO_2 doped with F or Cu ions have been controllably prepared by a one-step FSP method. Standard characterizations by BET, XRD, and TEM demonstrated the different type of dopants (either Cu or F) gave similar bulk crystal structure and morphological properties of the FSP-made TiO_2 in terms of surface area, crystallinity and phase composition, and morphology. However, the materials exhibited markedly different heterogeneous photocatalytic activity for the oxidation of gaseous ACE: F-doped TiO_2 exhibited the highest photocatalytic activity, while Cu-doped TiO_2 had a detrimental effect on the ACE photocatalytic oxidation. Comparative XPS studies confirmed they possessed identical elements' state (Ti, O, C) and surface bonding environment. By using high-field ^{1}H MAS NMR, this work clearly revealed the photocatalytic activity of the FSP-made TiO_2-based nanoparticles was governed by the distribution of surface hydroxyl groups on the TiO_2 surface. TiO_2 with a low number of surface terminal hydroxyl groups exhibited a high photocatalytic activity. This finding allows for a possible strategy to design high-performance photocatalysts for the target substrate by controlling the distribution of surface hydroxyl groups.

Acknowledgments

Financial support by the Australian Research Council through the ARC International Linkage Award with Boeing Company and UNSW Vice-Chancellor's Postdoctoral Research Fellowship is gratefully acknowledged. We are indebted to the UNSW Mark Wainwright Analytical Centre for use of their instruments and assistance from their staff, particularly Drs Bill Gong and Rasmus Linser.

Appendix A. Supplementary data

Supplementary data associated with this article can be found, in the online version, at http://dx.doi.org/10.1016/j.apcatb.2012.07.027.

References

[1] J. Mo, Y. Zhang, Q. Xu, J.J. Lamson, R. Zhao, Atmospheric Environment 43 (2009) 2229–2246.
[2] T. Sano, N. Negishi, K. Uchino, J. Tanaka, S. Matsuzawa, K. Takeuchi, Journal of Photochemistry and Photobiology A: Chemistry 160 (2003) 93–98.
[3] X. Chen, S.S. Mao, Chemical Reviews 107 (2007) 2891–2959.
[4] W. Choi, A. Termin, M.R. Hoffmann, Journal of Physical Chemistry 98 (1994) 13669–13679.
[5] J. Zhang, Q. Xu, Z. Feng, M. Li, C. Li, Angewandte Chemie International Edition 47 (2008) 1766–1769.
[6] J. Zhang, Q. Xu, M. Li, Z. Feng, C. Li, Journal of Physical Chemistry C 113 (2009) 1698–1704.
[7] E. McCafferty, J.P. Wightman, Surface and Interface Analysis 26 (1998) 549–564.
[8] G. Ertl, H. Knözinger, F. Schüth, J. Weitkamp, Handbook of Heterogeneous Catalysis, 2nd ed., Wiley-VCH, Weinheim, Germany, 2008.
[9] Q. Wang, M. Zhang, C. Chen, W. Ma, J. Zhao, Angewandte Chemie International Edition 49 (2010) 7976–7981.
[10] H. Zhang, H. Yu, A. Zheng, S. Li, W. Shen, F. Deng, Environmental Science and Technology 42 (2008) 5316–5321.
[11] J. Huang, N. van Vegten, Y. Jiang, M. Hunger, A. Baiker, Angewandte Chemie International Edition 49 (2010) 7776–7781.
[12] J. Huang, Y. Jiang, N. van Vegten, M. Hunger, A. Baiker, Journal of Catalysis 281 (2011) 352–360.
[13] W.Y. Teoh, R. Amal, L. Maedler, Nanoscale 2 (2010) 1324–1347.
[14] S.C. Kim, Journal of Hazardous Materials 91 (2002) 285–299.
[15] J. Araña, J.M. Doña-Rodrıǐguez, O. González-Dıǐaz, E. Tello Rendón, J.A. Herrera Melián, G. Colón, J.A. Navıĭo, J.P. Peña, Journal of Molecular Catalysis A: Chemical 215 (2004) 153–160.
[16] R. Kydd, W.Y. Teoh, J. Scott, D. Ferri, R. Amal, ChemCatChem 1 (2009) 286–294.
[17] H. Kim, W. Choi, Applied Catalysis B: Environmental 69 (2007) 127–132.
[18] J. Kim, W. Choi, H. Park, Research on Chemical Intermediates 36 (2010) 127–140.
[19] Y. Jiang, J. Huang, W. Dai, M. Hunger, Solid State Nuclear Magnetic Resonance 39 (2011) 116–141.
[20] L. Madler, H.K. Kammler, R. Mueller, S.E. Pratsinis, Journal of Aerosol Science 33 (2002) 369–389.
[21] S.L. Lee, J. Scott, K. Chiang, R. Amal, Journal of Nanoparticle Research 11 (2009) 209–219.
[22] W.Y. Teoh, L. Madler, D. Beydoun, S.E. Pratsinis, R. Amal, Chemical Engineering Science 60 (2005) 5852–5861.
[23] Y.K. Kho, W.Y. Teoh, L. Maedler, R. Amal, Chemical Engineering Science 66 (2011) 2409–2416.
[24] R. Strobel, S.E. Pratsinis, Journal of Materials Chemistry 17 (2007) 4743–4756.
[25] T. Ohno, K. Sarukawa, K. Tokieda, M. Matsumura, Journal of Catalysis 203 (2001) 82–86.
[26] Y.K. Kho, A. Iwase, W.Y. Teoh, L. Maedler, A. Kudo, R. Amal, Journal of Physical Chemistry C 114 (2010) 2821–2829.
[27] J.M. Coronado, S. Kataoka, I. Tejedor-Tejedor, M.A. Anderson, Journal of Catalysis 219 (2003) 219–230.
[28] R. Kydd, W.Y. Teoh, K. Wong, Y. Wang, J. Scott, Q.-H. Zeng, A.-B. Yu, J. Zou, R. Amal, Advanced Functional Materials 19 (2009) 369–377.
[29] J. Tang, H. Quan, J. Ye, Chemistry of Materials 19 (2006) 116–122.
[30] R. Asahi, T. Morikawa, T. Ohwaki, K. Aoki, Y. Taga, Science 293 (2001) 269–271.
[31] J.A.R. van Veen, F.T.G. Veltmaat, G. Jonkers, Journal of the Chemical Society, Chemical Communications (1985) 1656–1658.
[32] M.A. Henderson, Langmuir 12 (1996) 5093–5098.
[33] M. Crocker, R.H.M. Herold, A.E. Wilson, M. Mackay, C.A. Emeis, A.M. Hoogendoorn, Journal of the Chemical Society, Faraday Transactions 92 (1996) 2791–2798.
[34] M. Takeuchi, T. Kimura, M. Hidaka, D. Rakhmawaty, M. Anpo, Journal of Catalysis 246 (2007) 235–240.